Author(s): Zelený, M. & Sozinov, A. & Straka, L. & Björkman, T. & Nieminen, Risto M.

Title: First-principles study of Co- and Cu-doped Ni2MnGa along the tetragonal deformation path

Year: 2014

Version: Final published version

Please cite the original version:

Zelený, M. & Sozinov, A. & Straka, L. & Björkman, T. & Nieminen, Risto M. 2014. First-principles study of Co- and Cu-doped Ni2MnGa along the tetragonal deformation path. Physical Review B. Volume 89, Issue 18. 184103/1-9. ISSN 1550-235X (electronic). DOI: 10.1103/physrevb.89.184103.

First-principles study of Co- and Cu-doped Ni_2MnGa along the tetragonal deformation path

M. Zelený,[1,2] A. Sozinov,[3] L. Straka,[4] T. Björkman,[1] and R. M. Nieminen[1,5]

[1]*COMP/Department of Applied Physics, Aalto University School of Science, P.O. Box 11100, FI-00076 Aalto, Finland*

[2]*Institute of Materials Science and Engineering, NETME Centre, Faculty of Mechanical Engineering, Brno University of Technology, Technicka 2896/2, CZ-61669 Brno, Czech Republic*

[3]*Adaptamat Ltd, Yrityspiha 5, FI-00390 Helsinki, Finland*

[4]*Aalto University School of Engineering, Laboratory of Engineering Materials, PL 14200, FI-00076 Aalto, Finland*

[5]*Dean's office, Aalto University School of Science, P.O. Box 11000, FI-00076 Aalto, Finland*

(Received 14 August 2013; revised manuscript received 6 April 2014; published 7 May 2014)

The influence of Co and Cu doping on Ni-Mn-Ga Heusler alloy is investigated using the first-principles exact muffin-tin orbital method in combination with the coherent-potential approximation. Single-element doping and simultaneous doping by both elements are investigated in $Ni_{50-x}Co_xMn_{25-y}Ga_{25-z}Cu_{y+z}$ alloys, with dopant concentrations x, y, and z up to 7.5 at. %. Doping with Co in the Ni sublattice decreases the $(c/a)_{NM}$ ratio of the nonmodulated (NM) martensite, but it simultaneously increases the cubic phase stability with respect to the NM phase. Doping with Cu in the Mn or in Ga sublattices does not change the $(c/a)_{NM}$ ratio significantly and it decreases the cubic phase stability. For simultaneous doping by Co in the Ni sublattice and Cu in the Mn or Ga sublattices, the effects of the individual dopants are independent and about the same as for the single-element doping. Thus, the $(c/a)_{NM}$ ratio can be adjusted by Co doping while the phase stability can be balanced by Cu doping, resulting in stable martensite with a reduced $(c/a)_{NM}$. The local stability of the cubic phase with respect to the tetragonal deformation can be understood on the basis of a density-of-states analysis.

DOI: 10.1103/PhysRevB.89.184103 PACS number(s): 62.20.fg, 31.15.es, 75.50.Cc

I. INTRODUCTION

Much attention has been paid to the Ni-Mn-Ga magnetic shape memory (MSM) alloys in the scientific and engineering communities for their application potential in actuators, sensors, harvesters, and magnetic refrigeration systems [1–3]. An interesting phenomenon exhibited by the MSM alloys is a giant magnetic-field-induced strain (MFIS) of up to 12% [4], which is known also as the MSM effect or magnetically induced reorientation (MIR) [1–3]. The effect occurs by the motion of twin boundaries in twinned martensite microstructure or, in other words, by the rearrangement of twins, in an applied external magnetic field.

The prerequisite for the MFIS is the existence of a twinned martensite microstructure. This is generated by a temperature-induced martensitic phase transformation of a high-temperature cubic phase, austenite, to a low-temperature phase of lower symmetry, martensite [5,6]. For stoichiometric Ni_2MnGa, the martensitic transformation occurs at the temperature $T_M = 202$ K, whereas the Curie temperature T_C is about 376 K [7]. Several kinds of martensites have been observed in the Ni-Mn-Ga system [8,9]. The modulated five-layered (10M) phase exhibits about 6% MFIS [10,11], whereas nearly 10% MFIS can be obtained in the modulated seven-layered (14M) phase [12]. These values correspond to the maximum theoretical strains for MFIS allowed by the lattice distortion [1]. Both phases have c/a ratios smaller than 1.

Giant MFIS has never been reported for the third martensitic Ni-Mn-Ga phase (see Ref. [4] and references therein) which has a purely tetragonal lattice without modulation [nonmodulated (NM) martensite] and a $(c/a)_{NM} \approx 1.17$–1.23 [13]. However, a MFIS of 12% has recently been reported in the NM phase for a structure with reduced $(c/a)_{NM} = 1.147$, achieved by simultaneous doping by 4 at. % of Cu and Co [4] resulting in the alloy composition $Ni_{46}Co_4Mn_{24}Ga_{22}Cu_4$. The large MFIS was made possible by the lowered twinning stress, which seems to be related to the reduced value of $(c/a)_{NM}$. Doping also had an effect on T_M and T_C: both temperatures were above room temperature, $T_M = 330$ K and $T_C = 393$ K, which improves the practical applicability of the material.

The effect of compositional changes in Ni-Mn-Ga alloys and doping by different elements have been studied intensively in the recent decade by experimental and theoretical techniques and have been summarized in several reviews [14–17]. One of the important reasons for the alloy doping and composition adjustments is the increase of the operating temperature of the MSM material by shifting T_M and T_C to high temperatures. For example, when the concentration of Ni is increased in the Ni-Mn-Ga alloy, the T_M also increases [18,19]. For the Co- and Cu-doped alloys deficient in Mn or Ga, T_M increases [20,21], but it decreases if Co or Cu replaces Ni atoms [14,23]. On the other hand, the addition of Co instead of Ni increases the T_C. Here, we focus on simultaneous Cu and Co doping as this case has been shown recently to be crucial for keeping both T_M and T_C high and for the existence of MSM effect in the NM phase [4].

On the basis of the *ab initio* band-structure calculations, the Jahn-Teller effect has been proposed as responsible for structural instability of the austenite phase [22,24–26]. This effect is closely related to the Fermi surface nesting and phonon mode softening, which were revealed for the cubic phase [27–29]. Also, the exchange interaction between the Mn atoms is likely of high importance for structural properties of Ni-Mn-Ga alloys [17]. Unfortunately, the general mechanism of these effects has not been yet completely clarified.

Many theoretical works based on *ab initio* calculations have been dedicated to off-stoichiometric or doped Ni-Mn-Ga alloys, with special attention to site preference and elastic constants. For most of the off-stoichiometric Ni_2MnGa, the

normal site preference is predicted, i.e., the excess atoms of the rich component prefer to occupy the sublattice of the deficient element [29]. The site preference problem of doping elements has been successfully clarified also for Cu and Co doping: Co exhibits a strong tendency to occupy the Ni sublattice in all types of alloys and Cu atoms always occupy the sublattice of the host elements in deficiency [26].

The works dedicated to the calculation of elastic constants have focused mainly on the high-temperature cubic phase and their correlations with T_M since T_M usually decreases with increasing C' [30]. An empirical rule also follows from experiments: a larger number of valence electrons per atom (e/a) corresponds to a higher T_M [18,31–33]. The energy difference between the austenite and the nonmodulated martensite phase $\Delta E_{A\text{-NM}}$ is another quantity closely related to T_M that can be easily obtained from *ab initio* calculations. Its comparison with experimentally determined T_M shows that a larger difference in total energies corresponds to a higher T_M [34]. A comparative study for the total energy differences between austenite and the NM phase is still missing for (Cu- and Co-) doped Ni-Mn-Ga alloys, despite the importance of this quantity for understanding the phase stability in these systems.

The purpose of this paper is to reveal how the Co and Cu doping influences the stability of austenite with respect to NM martensite and also its effect on the equilibrium $(c/a)_{\text{NM}}$ ratio of NM martensite. We present a detailed and comprehensive first-principles investigation of the effects of Co and Cu doping, studying first doping by single element and then simultaneous doping by both elements. Special attention is paid to the latter case, i.e., to Ni-Mn-Ga-Co-Cu alloys, since these exhibit new and interesting properties [4] but have not previously been studied theoretically and published experimental results are rare. We find that previously known empirical rules to an extent can be accounted for by a density-of-states (DOS) analysis. This study presents an attempt to understand the Ni-Mn-Ga-Co-Cu alloys theoretically and as such it can not provide complete answers to all questions on these new alloys, e.g., properties of modulated structures or nature of low twinning stress. Nonetheless, we believe that the presented results are of high relevance for the design of new compositions and provide a firm base for further more detailed theoretical work.

II. COMPUTATIONAL METHODS

All calculations of this work were carried out by the use of the first-principles method formulated with the exact muffin-tin orbital (EMTO) method [35–37]. In combination with the full charge density (FCD) technique for total energy calculations [35], the EMTO method is also suitable to accurately describe the total energy with respect to anisotropic lattice distortions such as tetragonal deformation. The chemical disorder caused by doping elements was included by using of the coherent-potential approximation (CPA) [38,39]. This approximation does not take into account short-range interactions around the doping atoms, however, in full Heusler alloys, such short-range interactions only have a small influence on the electronic structure [40]. The exchange correlation was described using the Perdew-Burke-Ernzerhof (PBE) generalized gradient approximation [41], and the scalar-relativistic and soft-core approximations were employed. The s, p, d, and f orbitals were included in the EMTO basis sets. The Ni $3d^8 4s^2$, Mn $3d^5 4s^2$, Ga $3d^{10} 4s^2 4p^1$, Co $3d^7 4s^2$, and Cu $3d^{10} 4s^1$ were treated as valence states. The Green's function was calculated for 32 complex energy points distributed exponentially on a semicircular contour. In order to obtain the best agreement with experiments for a $(c/a)_{\text{NM}}$, we introduced an additional optimization of the muffin-tin potential on the Ni sublattice according to Refs. [16,42] by choosing the atomic radius $R_{ws}^{\text{Ni}} = 1.10 R_{ws}$ and overlapping potential spheres $R_{mt}^{\text{Ni}} = 0.95 R_{ws}$, where R_{ws} is the average Wigner-Seitz radius. For the other sublattices, the usual setup $R_{mt} = R_{ws}$ was used. In the one-center expansion of the full charge density, the number of components was truncated at 8. The Brillouin zone was sampled by a $13 \times 13 \times 13$ uniform k-point mesh without any smearing technique.

For stoichiometric Ni_2MnGa, the described settings resulted in the lattice constant of austenite ($L2_1$ structure) equal to 5.813 Å and local magnetic moments 0.33 μ_B and 3.52 μ_B of Ni and Mn atoms, respectively. For the NM phase, we obtained the lattice constant $a_{\text{NM}} = 5.382$ Å, $(c/a)_{\text{NM}} = 1.256$, and local magnetic moments 0.38 μ_B for Ni and 3.42 μ_B for Mn. These results are in good agreement with previous calculations (see Table 6.1 in Ref. [43] and references therein). The agreement for the lattice parameter of austenite is also very good compared to the experimental value $a_A = 5.825$ Å [8,24]. The experimental lattice parameter of martensite $a_{\text{NM}} = 5.520$ Å is slightly larger [8,24] than our calculated value. The calculated equilibrium $(c/a)_{\text{NM}}$ ratio is overestimated compared to experimental value $(c/a)_{\text{NM}} = 1.17$ [8], which is, however, usual for all first-principles calculations [15,17,43–45].

After careful analysis of previous theoretical studies and available experimental results, three types of doping were considered: Co in Ni sublattice and Cu in Mn or Ga sublattices with dopant concentrations x, y, and z between 0% and 7.5% in $Ni_{50-x}Co_xMn_{25-y}Ga_{25-z}Cu_{y+z}$ alloys. For all such combinations, we calculated a series of total energies as a function of c/a in the range between $c/a = 0.9$ and 1.4 at constant volume, which describes the tetragonal deformation of austenite phase with $L2_1$ structure ($c/a = 1$). All calculated total energies along the deformation path are related to the energy of cubic structure for alloy with given composition. This provides a clear picture about the effect of doping elements on equilibrium $(c/a)_{\text{NM}}$ and relative energy difference $\Delta E_{A\text{-NM}}$ between austenite and the NM phase.

III. RESULTS

A. Equilibrium volume and magnetic moments

We started the investigation by estimating the equilibrium atomic volumes of austenite V_{0A} and tetragonal NM martensite $V_{0\text{NM}}$. This is important for correct calculations of total energies since they depend on the equilibrium atomic volume. Our results for austenite with single-element doping show a linear decrease of atomic volume with increasing dopant concentration, which is in agreement with previously published data [26]. For combined two-element doping, the

TABLE I. The local magnetic moments (in μ_B) of Ni, Mn, and Co in austenite and martensite phases for nondoped $Ni_{50}Mn_{25}Ga_{25}$ and for alloys with dopant concentrations x, y, or z equal to 5% or 7.5%. The columns with equilibrium $(c/a)_{NM}$ and relative change of equilibrium volume with respect to volume of austenite ΔV_{rel} (in %) are also included for the martensite phase.

	Austenite			Nonmodulated martensite				
Composition	Ni	Mn	Co	Ni	Mn	Co	$(c/a)_{NM}$	ΔV_{rel}
$Ni_{50}Mn_{25}Ga_{25}$	0.33	3.52		0.38	3.42		1.256	−0.32
$Ni_{42.5}Co_{7.5}Mn_{25}Ga_{25}$	0.35	3.45	1.03	0.39	3.42	0.93	1.164	−0.10
$Ni_{50}Mn_{25}Ga_{17.5}Cu_{7.5}$	0.39	3.50		0.38	3.46		1.251	−0.31
$Ni_{50}Mn_{17.5}Ga_{25}Cu_{7.5}$	0.26	3.53		0.30	3.48		1.217	−0.10
$Ni_{45}Co_5Mn_{25}Ga_{17.5}Cu_{7.5}$	0.42	3.45	1.09	0.38	3.41	0.84	1.201	−0.27
$Ni_{42.5}Co_{7.5}Mn_{25}Ga_{20}Cu_5$	0.40	3.43	1.06	0.39	3.40	0.87	1.178	−0.23

decrease is much larger but still linear, giving the following simple rule for prediction of equilibrium volume (in Å^3) of austenite:

$$V_{0A} = V_{0A}^* - 0.0092x - 0.0155y - 0.0207z, \qquad (1)$$

where V_{0A}^* is the atomic volume of $Ni_{50}Mn_{25}Ga_{25}$ without any doping, x is the concentration of Co at Ni sites, y is the concentration of Cu at Mn sites, and z is the concentration of Cu at Ga sites, for the studied $Ni_{50-x}Co_xMn_{25-y}Ga_{25-z}Cu_{y+z}$ alloy. This rule is valid for the whole concentration range used in this study. The volume decrease can be simply explained by the size difference between the host and alloying elements, with the exception of Co at Ni sites where magnetic effects probably affect the volume [26].

The equilibrium volume of the NM phase V_{0NM} is even smaller than V_{0A}, but the situation is slightly complicated. The concentration dependencies are still almost linear, but they follow a different rule, with the largest deviation being observed for Co doping. The reduction of volume is not as strong as in the case of austenite and V_{0NM} is somewhat larger than expected. This is probably due to the decreased equilibrium $(c/a)_{NM}$ of these alloys (see below), which pushes V_{0NM} higher. Similar trends are found in all other compositions containing Co but less significantly so.

The study of equilibrium volumes brings another finding. Although the energies along the tetragonal deformation path depend on atomic volume, their differences at V_{0A} and V_{0NM} at the same composition are very small, especially for the small dopant concentrations ($x,y,z \lesssim 2.5\%$). Thus, these volume differences were neglected and the total energies were calculated at average volume between the V_{0A} and V_{0NM} of alloy with given composition in all following calculations.

Similar linear trends are found also for the magnetic moments of austenite. However, the local magnetic moments do not differ more than about 0.1 μ_B in whole concentration range compared to nondoped $Ni_{50}Mn_{25}Ga_{25}$. The NM phase does not exhibit such strictly linear dependencies, which is caused by the varying equilibrium $(c/a)_{NM}$ for different concentrations. The magnetic moments of Co in this phase are ~0.2 μ_B smaller than for the austenite phase. The local magnetic moments for Ni, Mn, and Co atoms are summarized in Table I for selected compositions. The table displays values for nondoped $Ni_{50}Mn_{25}Ga_{25}$ alloy and alloys where concentration of one of the doping elements is equal to 7.5%, which is the highest concentration used in this study.

B. Single-element doping: Ni-Mn-Ga-Cu and Ni-Mn-Ga-Co alloys

First, we discuss Cu doping on Ga deficient alloy, i.e., the case where Cu atoms occupy the Ga sites. Figure 1(a) shows the total energy as a function of tetragonal ratio c/a

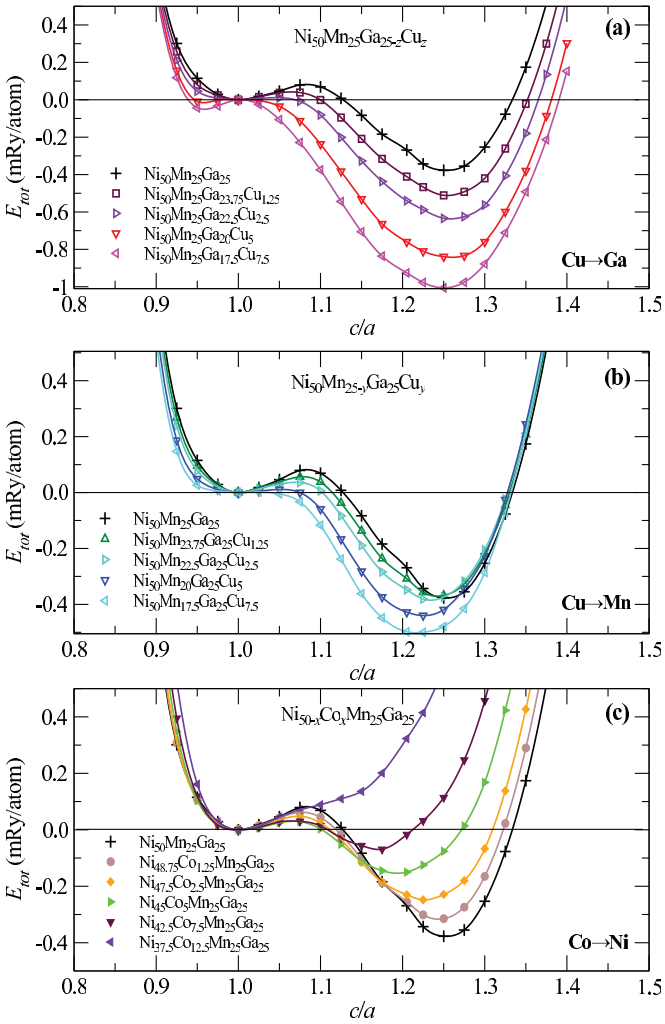

FIG. 1. (Color online) Total energy as a function tetragonal ratio c/a for alloys with different concentration of Cu in the Ga sublattice (a), Cu in the Mn sublattice (b), and Co in the Ni sublattice (c). All energies are related to the energy of the cubic structure of alloy with given composition.

for $Ni_{50}Mn_{25}Ga_{25-z}Cu_z$ alloys with tetragonally deformed $L2_1$ structure with z between 0 and 7.5%. It can be seen from the figure that the Cu doping stabilizes the martensite phase because the minima corresponding to the NM phases are much deeper than for nondoped $Ni_{50}Mn_{25}Ga_{25}$ and $\Delta E_{A\text{-NM}}$ increases with increasing Cu concentration. For nondoped $Ni_{50}Mn_{25}Ga_{25}$, the $\Delta E_{A\text{-NM}}$ is equal to 0.379 mRy/atom (5.16 meV/atom). The increasing of the $\Delta E_{A\text{-NM}}$ approximately corresponds to 0.090 mRy/atom (1.22 meV/atom) for each 1% of added Cu. Because the experiments reveal that added Cu increase the T_M and stabilize the NM phase [20,21], our result supports the previous theoretical finding for nondoped off-stoichiometric Ni-Mn-Ga alloys, that a larger $\Delta E_{A\text{-NM}}$ corresponds to a higher T_M [34]. Addition of Cu has only a small effect on the position of equilibrium c/a, which stays almost unchanged or even slightly increases for a small concentration z [Fig. 1(a)].

For Cu doping at Mn sites (general formula $Ni_{50}Mn_{25-y}Ga_{25}Cu_y$), the alloy behaves differently, as shown in Fig. 1(b). The $(c/a)_{\text{NM}}$ slightly decreases with increasing Cu concentration. Surprisingly, this effect is weaker for larger y. The effect on the $\Delta E_{A\text{-NM}}$ is also very weak. The energy of NM martensite remains almost unchanged or even increases for y up to 2.5%. For larger y, the effect is more significant and the energy of the NM phase goes down, but still less than in the case of Ga deficient alloys. The effect of Cu on $\Delta E_{A\text{-NM}}$ is approximately two times stronger for Cu atoms at Ga sites than for Cu atoms at Mn sites. These results are in good agreement with a recently published study about Cu doping in Ni_2MnGa alloys, where a supercell approach was used and chemical disorder was not taken into account [46].

Co doping at Ni sites ($Ni_{50-x}Co_xMn_{25}Ga_{25}$) has a much stronger effect on the equilibrium $(c/a)_{\text{NM}}$ [Fig. 1(c)] and even a low concentration of Co decreases $(c/a)_{\text{NM}}$ significantly and also noticeably decreases $\Delta E_{A\text{-NM}}$. For alloys with the composition $Ni_{45}Co_5Ni_{25}Mn_{25}$ the values are $(c/a)_{\text{NM}} = 1.191$ and $\Delta E_{A\text{-NM}} = 0.152$ mRy/atom (2.07 meV/atom). If the concentration of Co is too high ($x \gtrsim 9\%$), the NM phase becomes less stable than austenite and a further increase of Co concentration results in unstable NM phase. This corresponds to the experimental result that increasing Co concentration stabilizes the cubic phase and decreases the T_M [14,23].

From the shape of the tetragonal deformation curves it can be seen that all types of doping lower the barrier between the austenite and martensite phases (Fig. 1). For doping by Cu, the barrier drops to zero for $y \approx 6\%$ and $z \approx 4\%$. A new energy local minimum develops at $c/a < 1$ for $z > 4\%$ [see Fig. 1(a)]. The absence of a barrier means that the cubic phase loses its metastability, and becomes unstable at 0 K. It should be noted that vanishing of the barrier can involve also increasing of stability of the modulated phase with $c/a < 1$, but that problem is beyond the scope of this study. The height of the barrier measured from the cubic phase minimum is least affected by Co doping, where the barrier still exists even for higher x, where the austenite is a stable phase and the tetragonal martensite is metastable, although the barrier of course vanishes when the martensitic energy minimum is completely destabilized.

C. Two-element doping: Ni-Mn-Ga-Co-Cu alloys

From the single-element doping results presented above and from the experiments and reasoning in Ref. [4] it follows that a decrease in T_M by Co doping performed in order to decrease c/a can be compensated by simultaneous doping by Cu. We carried out calculations for simultaneous doping by Cu and Co to understand in which way the effects of individual elements are combined. Here, we present in detail only the case with Co at Ni sites and Cu at Ga sites since Cu at Ga sites appears to have a stronger effect. From the results presented in the following, it can be seen that the effects of Co and Cu are quite independent and the overall effect can be estimated rather precisely using linear superposition of the effects obtained by single-element doping.

Figure 2(a) shows the total energy of the $Ni_{45}Co_5Mn_{25}Ga_{25-z}Cu_z$ alloy as a function of tetragonal ratio c/a for different values of z. It is obvious that the decrease of $\Delta E_{A\text{-NM}}$ arising from doping by 5% of Co is now compensated by Cu doping since the energy of NM phase decreases and $\Delta E_{A\text{-NM}}$ grows. For example, the $Ni_{45}Co_5Mn_{25}Ga_{20}Cu_5$ alloys has $\Delta E_{A\text{-NM}} = 0.437$ mRy/atom (5.94 meV/atom), whereas the $\Delta E_{A\text{-NM}}$ of $Ni_{45}Co_5Mn_{25}Ga_{25}$ alloys (no Cu doping) is smaller by 0.285 mRy/atom (3.88 meV/atom). On the other hand, the equilibrium $(c/a)_{\text{NM}}$ is smaller due to the Co presence, but remains almost the same (1.190–1.200) for

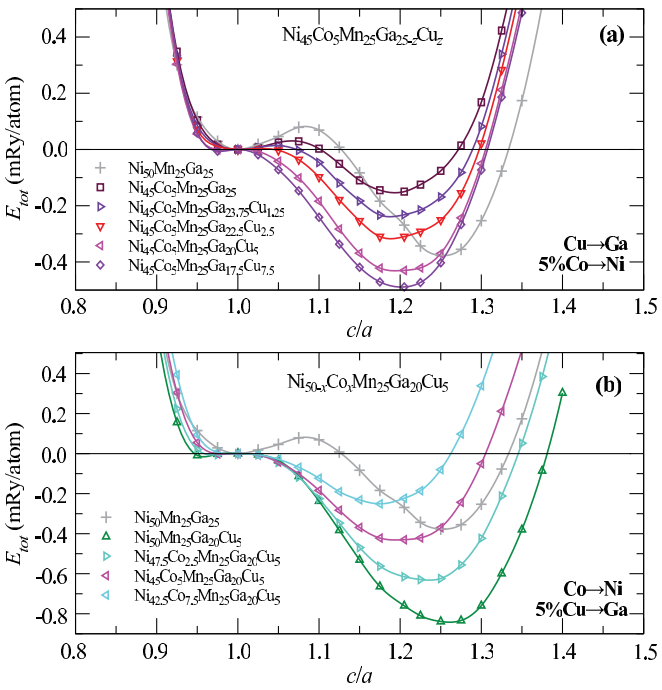

FIG. 2. (Color online) Total energy as a function of the tetragonal ratio c/a for simultaneously doped alloys with different concentrations z of Cu in the Ga sublattice and constant concentration 5% of Co in the Ni sublattice (a), and different concentration x of Co in the Ni sublattice and constant concentration 5% of Cu in the Ga sublattice (b). All energies are related to the energy of the cubic structure of an alloy with the given composition. For comparison, a light gray curve corresponding to nondoped $Ni_{50}Mn_{25}Ga_{25}$ is also shown.

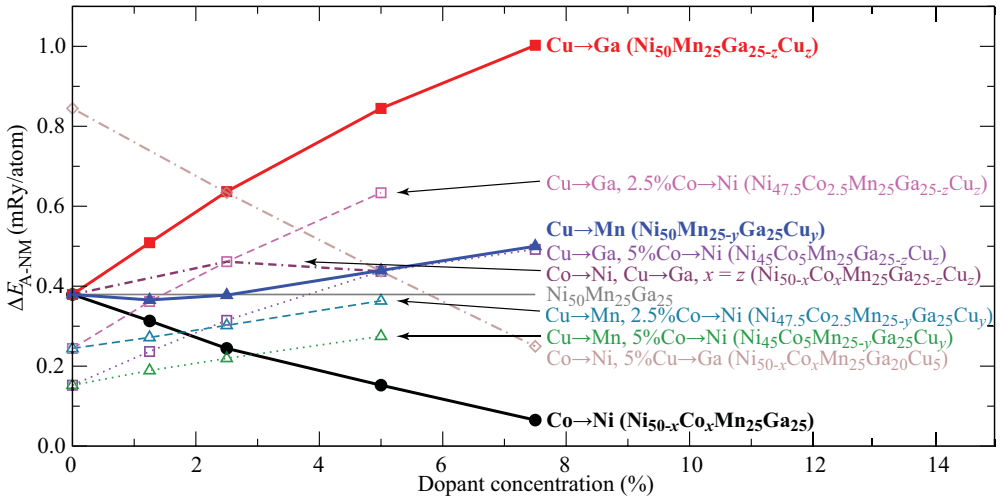

FIG. 3. (Color online) Total energy differences between the austenite and NM phases $\Delta E_{A\text{-NM}}$ as a function of dopant concentration x, y or z for different alloy compositions. The horizontal thin line corresponds to values for the nondoped Ni-Mn-Ga alloy.

all displayed curves, because the Cu itself has a negligible effect on $(c/a)_{\text{NM}}$.

A similar linear superposition of the effects of Cu and Co can be seen also for alloys with the general composition $Ni_{50-x}Co_xMn_{25}Ga_{20}Cu_5$. The total energies as a function of c/a are shown in Fig. 2(b) for the case where the concentration of Cu in the Ga sublattice is constant and the concentration of Co grows. Here, the energy difference $\Delta E_{A\text{-NM}}$ strongly decreases with increasing concentration of Co and simultaneously the equilibrium $(c/a)_{\text{NM}}$ decreases. $\Delta E_{A\text{-NM}}$ of the alloy $Ni_{45}Co_5Mn_{25}Ga_{20}Cu_5$ is smaller by 0.408 mRy/atom (5.55 meV/atom) than for $Ni_{50}Mn_{25}Ga_{20}Cu_5$ (without Co doping). However, both values are still larger than the value for nondoped $Ni_{50}Mn_{25}Ga_{25}$ due to the presence of Cu in the Ga sublattice.

Since all mentioned types of doping decrease the barrier between the austenite and the NM phase, the effect is correspondingly stronger for simultaneous doping by Co and Cu. The barrier vanishes for concentrations higher than ∼2.5% of each doping element.

D. Distribution of Cu between Mn and Ga sublattices

The properties of the NM phase depend on the Cu distribution between Ga and Mn sites. This effect cannot be neglected because the difference in total energies of NM phase for edge cases is as large as 0.405 mRy/atom (5.50 meV/atom) for 5% of Cu in the alloy. The dependence of $\Delta E_{A\text{-NM}}$ on the Cu distribution between the sites is linear with a minimum for all Cu at Mn sites and and maximum for all Cu at Ga sites. The effect is weaker for two-element doping when Co also resides at the Ni sites. The effect of the Cu distribution on $(c/a)_{\text{NM}}$ is very weak, with Cu at Mn sites decreasing the $(c/a)_{\text{NM}}$ slightly and Cu at Ga sites almost having no effect at all. Alloying with 5% of Cu only causes a difference in $(c/a)_{\text{NM}}$ of 0.038 and additional Co doping further reduces the effect.

IV. DISCUSSION

The calculated results for $\Delta E_{A\text{-NM}}$ and $(c/a)_{\text{NM}}$ are summarized in Figs. 3 and 4. $\Delta E_{A\text{-NM}}$ decreases with increasing Co concentration at Ni sites and increases with increasing Cu

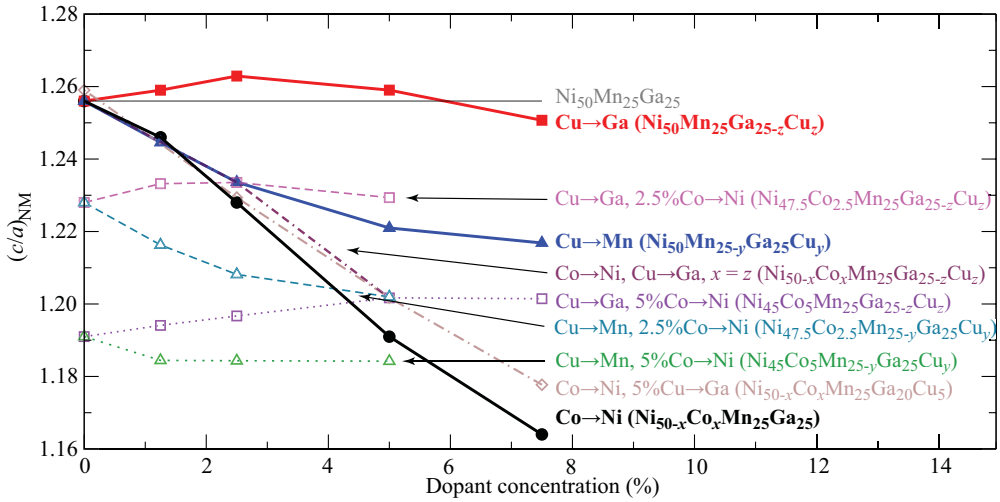

FIG. 4. (Color online) Equilibrium tetragonal ratio of the NM phase $(c/a)_{\text{NM}}$ as a function of dopant concentration x, y, or z for different alloy composition. The horizontal thin line corresponds to the $(c/a)_{\text{NM}}$ for the nondoped Ni-Mn-Ga alloy.

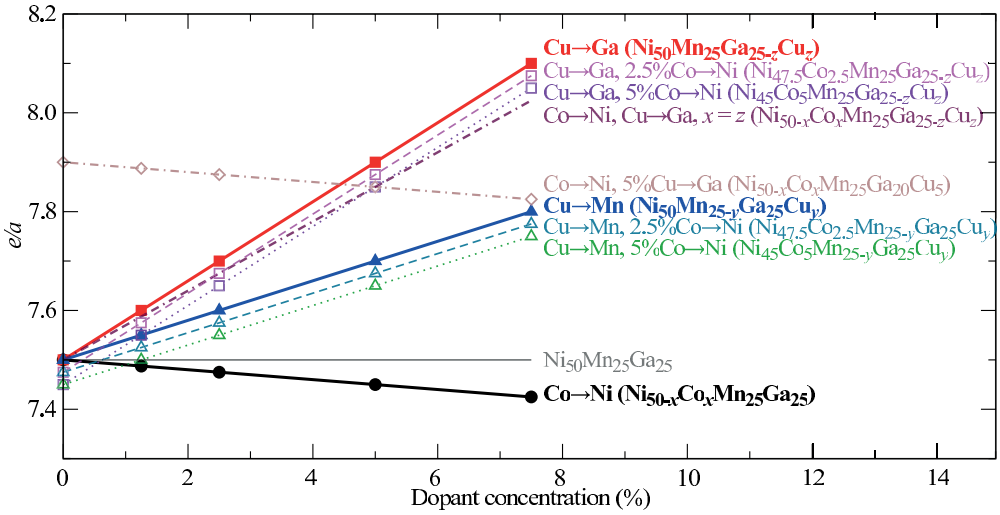

FIG. 5. (Color online) Number of valence electrons per atom e/a as a function of dopant concentration x, y, or z for different alloy compositions. The horizontal thin line corresponds to values for the nondoped Ni-Mn-Ga alloy.

concentration at Ga sites (Fig. 3). These trends can be seen also for combined two-element doping, with the contribution from each element approximately corresponding to its effect in single-element doping. The effect of Cu slightly dominates because the same concentrations of both doping elements increase $\Delta E_{A\text{-NM}}$ over the value for nondoped Ni-Mn-Ga. When Cu occupies Mn sites, $\Delta E_{A\text{-NM}}$ slightly decreases at first and then increases with increasing Cu concentration.

The results are in agreement with experimental findings, which show that Co at Ni sites decreases the T_M [14] and Cu at Mn or Ga sites increases T_M [20,21]. The previously published rule for off-stoichiometric, nondoped Ni-Mn-Ga alloys, which says that T_M is correlated with $\Delta E_{A\text{-NM}}$, is valid also in the case of doped Ni-Mn-Ga alloys [34]. Our results also reflect the empirical rule that T_M, and consequently $\Delta E_{A\text{-NM}}$, should grow with increasing e/a [18,31–33]. This quantity is shown in Fig. 5 for the same alloys as in Fig. 3. The only deviation from the empirical rule can be seen for small concentrations of Cu at Mn sites, the e/a grows but $\Delta E_{A\text{-NM}}$ decreases or remains the same, and only for larger y, $\Delta E_{A\text{-NM}}$ increases. Our results also agree with the previous theoretical finding that the tetragonally distorted structure is preferred in Heusler alloys only above certain $e/a > 7.25$–7.5 [47], while the cubic structure is preferred below this e/a ratio. In our particular case, the cobalt doping decreases the e/a, which results in unstable tetragonal structure when crossing the point $e/a \approx 7.4$.

Note that that for the calculation of e/a, a different number of valence electrons was used than we have introduced in Sec. II as an input for EMTO calculations. In previous studies, only the $4s^2 4p^1$ orbitals were treated as valence states of Ga and $3d^{10}$ electrons were not included in this case [20,33]. For other elements, the number of valence electrons was the same as described in Sec. II.

Almost all compositions studied in this work decrease the equilibrium $(c/a)_{\text{NM}}$ below the value for the nondoped alloy (Fig. 4), only simple doping by Cu in the Ga sublattice will increase it for small Cu concentrations, but for larger z, the value of $(c/a)_{\text{NM}}$ is also smaller than for the nondoped alloy. A strong decrease can be seen for Co doping on Ni sites. If Cu is added instead of Ga to the alloy with Co, the $(c/a)_{\text{NM}}$ increases, but never exceeds the value for the nondoped alloy. For alloys with the same concentration of doping elements ($Ni_{50-x}Co_xMn_{25}Ga_{25-z}Cu_z$, where $x = z$), the dependency is very similar to that of alloys with the compositions $Ni_{50-x}Co_xMn_{25}Ga_{25}$ or $Ni_{50-x}Co_xMn_{25}Ga_{20}Cu_5$, meaning that the effect of Co doping is fundamental for determination of $(c/a)_{\text{NM}}$.

The effect of doping on the local stability of the austenite phase with respect to the tetragonal deformation (tetragonal shear modulus C' softening or hardening) can be explained by an analysis of a pseudogap in the minority (spin-down) DOS about 0.05 Ry below the Fermi level E_f and a small peak about 0.02 Ry below the E_f. The pseudogap arises from the covalent nature of bonding between Ni and Ga [48], whereas the peak is related to a Jahn-Teller instability. This peak splits when a tetragonal deformation is exerted on the $L2_1$ structure, which leads to a decrease of the DOS at the Fermi level E_f [see Fig. 6(a)] and stabilization of the tetragonal martensite phase [22,24,49–51]. Li *et al.* showed that doping by Co in the Ni sublattice and Cu in the Mn and Ga sublattices fills the pseudogap and decreases this peak in the cubic phase, which leads to a weaker Jahn-Teller instability. Furthermore, a shallower and narrower pseudogap compared to the Ni_2MnGa indicates a weaker covalent bonding. The overall stability of the austenite with respect to the tetragonal deformation is a result of competition between both described effects [26].

Additionally, the position of the energy barrier on the tetragonal deformation path is also related to the position of the Jahn-Teller peak with respect to the E_f. When the tetragonal distortion pushes the peak through the Fermi level, the DOS at E_f initially increases, raising the energy until the peak is centered on E_f [see Fig. 6(a)]. This corresponds to the top of the barrier. Further tetragonal deformation will again reduce the DOS at E_f which makes tetragonal distortion energetically favorable. If the suppression of the Jahn-Teller effect by doping is very strong, the DOS at E_f never grows up upon tetragonal deformation which results in a very flat profile of total energy

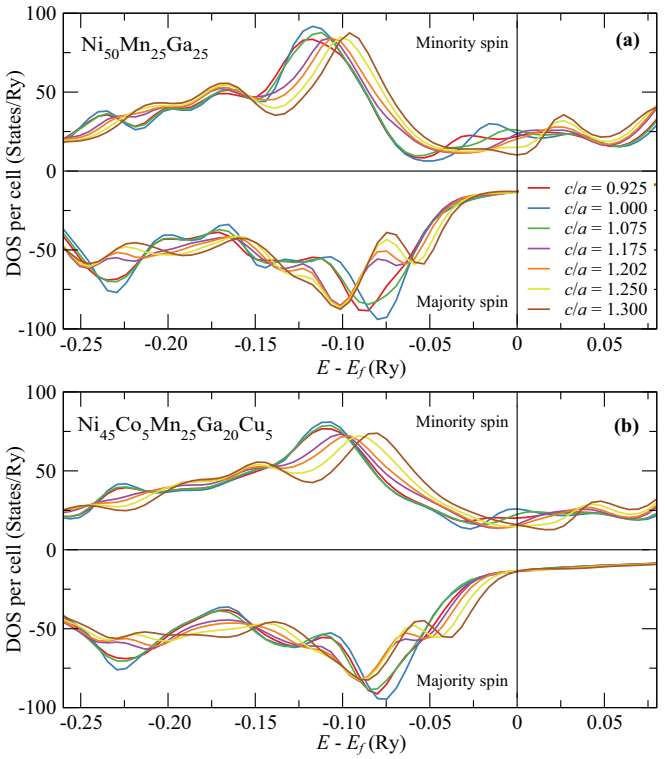

FIG. 6. (Color online) The density of states for $Ni_{50}Mn_{25}Ga_{25}$ (a) and $Ni_{45}Co_5Mn_{25}Ga_{20}Cu_5$ (b) alloys in different states along the tetragonal deformation path. The zero energy corresponds to the Fermi level E_f.

around $c/a = 1$ and the barrier does not exist. In some cases, the change in number of electrons compared with the undoped case shifts the Fermi level very close to the peak or even below it [see Fig. 6(b)]. This shift of the peak results in a new position of the barrier closer to the cubic phase or it can even completely destabilize the cubic phase with respect to the tetragonal deformation.

The considerations related to the Jahn-Teller effect and the energy barrier are valid only near the austenite equilibrium geometry (around $c/a = 1$). The stability of the NM phase is affected also by other modifications of the electronic structure occurring far below E_f (Fig. 6).

Figure 7 shows in detail our results for the minority (spin-down) DOS channel around E_f for the cubic $L2_1$ austenite state without dopants and for a concentration of 5% of doping elements. All studied dopings decrease the peak size, with the strongest effect for Co at Ni sites and smallest effect for Cu doped in Ga sublattice. Also, the peak position with respect to E_f is changed, with the largest effect coming, in contrast, from Cu at Ga sites. Effect of doping on pseudogap shallowing and narrowing is weakest for Cu in the Ga site, but strongest for Cu in the Mn site.

When Cu is doped in the Ga sublattice, the shift of the Fermi level closer to the peak is very strong (filled red triangles in Fig. 7), thus enhancing the contribution of the Jahn-Teller effect to local destabilization of austenite (C' softening) [26] and also shifts the position of the barrier closer to the cubic phase, which results, for higher concentration of Cu, in absolute instability of cubic phase with respect to the

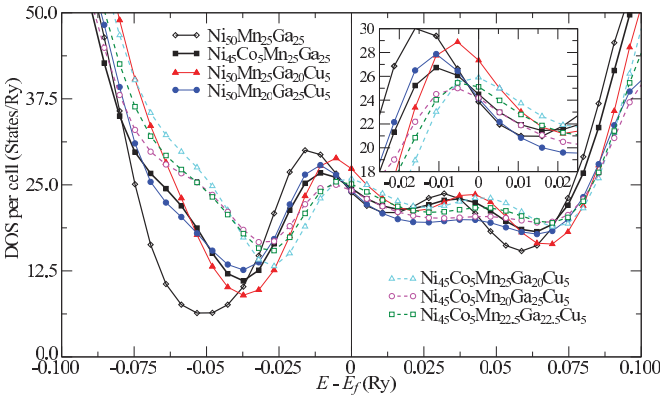

FIG. 7. (Color online) The density of states for the minority (spin-down) channel of different Ni-Mn-Ga alloys in the cubic austenite phase. The zero energy corresponds to the Fermi level E_f. The inset graph shows the DOS around E_f in detail.

tetragonal deformation and stabilization of a new structure with $c/a < 1$ [Fig. 1(a)].

Because all kinds of doping reduce the Jahn-Teller instability and fill the pseudogap, these effects are even more pronounced for simultaneous doping by both elements (open symbols in Fig. 7). As we mentioned above, the effects of each doping element are quite independent. However, the narrowing and shallowing of the pseudogap is more pronounced by doping than the reduction of the Jahn-Teller peak. It means that the local stability of the austenite phase with respect to the tetragonal deformation will be always reduced compared to nondoped Ni_2MnGa alloy. That corresponds to C' softening, which is seen from the more flat profile of energy around $c/a = 1$ in Fig. 7. On the other hand, the Jahn-Teller effect still persists and the E_f is shifted closer to the Jahn-Teller peak, which pushes the barrier on the tetragonal deformation path closer to the cubic structure. This effect is similar to the case when only Cu is used for doping in the Ga sublattice.

V. CONCLUSIONS

The Co and Cu doping of Ni-Mn-Ga Heusler alloys has been studied using the EMTO-CPA first-principles method. For Cu doping of a Ga-deficient alloy, we have found a strong increase in the energy difference between the austenite and the nonmodulated martensite phase $\Delta E_{A\text{-NM}}$, but just a small change of equilibrium $(c/a)_{\text{NM}}$ of nonmodulated martensite. If, on the other hand, Cu is instead doped at Mn sites, the increase of $\Delta E_{A\text{-NM}}$ is much smaller and a slight decrease of $(c/a)_{\text{NM}}$ is seen. Co doping at Ni sites has much stronger effects, with increasing concentration of Co strongly decreasing both $\Delta E_{A\text{-NM}}$ and $(c/a)_{\text{NM}}$. These theoretical results are in good agreement with previous experimental findings because Cu doped in the Ga or Mn sublattice will increase the martensitic transformation temperature T_M and Co in the Ni sublattice will decrease it. $\Delta E_{A\text{-NM}}$ can be used as a qualitative indicator of T_M also for doped Ni-Mn-Ga alloys and not only for off-stoichiometric alloys. Our results also correspond to another empirical rule, namely, that both T_M and $\Delta E_{A\text{-NM}}$ are correlated with the number of valence electrons per atom e/a in the alloy.

We have also investigated alloys where both elements Cu and Co were used in simultaneous doping. Our results show that the effects of simultaneous doping can be estimated using a linear superposition of the effects of individual dopants. This can be used for effective tuning of material properties; in particular, the decreasing of $\Delta E_{A\text{-NM}}$ (and T_M) arising from Co doping can be compensated by Cu doping at Ga sites. However, the reduction of $(c/a)_{\text{NM}}$ due to the Co doping is preserved because the Cu doping has just a small effect on this quantity.

We have also analyzed the density of states to explain the stability of austenite state with respect to the tetragonal distortion and to explain the position of a barrier on the deformation path. The position of the barrier depends on the position of the peak related to the Jahn-Teller instability with respect to the Fermi level because it is influenced by the doping elements. The shift of the peak closer to the Fermi level results in the shift of the top of the barrier closer to the cubic structure.

ACKNOWLEDGMENTS

This research has been supported by the Academy of Finland through the Center of Excellence Program (2012–2017) and postdoctoral researcher Grant No. 134002, and the European Regional Development Fund in the framework of the research project NETME Centre (Project No. CZ. 1.05/2.1.00/01.0002) under the Operational Programme Research and Development for Innovation. The access to the CERIT-SC computing and storage facilities provided under the programme Center CERIT Scientific Cloud, part of the Operational Program Research and Development for Innovations, Reg. No. CZ. 1.05/3.2.00/08.0144 and computational resources from the Finland IT Center for Science (CSC) and the Aalto Science-IT project is highly acknowledged. We thank L. Vitos for helpful discussions regarding the settings of the EMTO-CPA computational code.

[1] O. Söderberg, Y. Ge, A. Sozinov, S.-P. Hannula, and V. K. Lindroos, in *Handbook of Magnetic Materials*, edited by K. H. J. Buschow (Elsevier, Amsterdam, 2006), Vol. 16, pp. 1–39.

[2] O. Heczko, N. Scheerbaum, and O. Gutfleisch, in *Nanoscale Magnetic Materials and Applications*, edited by J. Liu, E. Fullerton, O. Gutfleisch, and D. Sellmyer (Springer, Berlin, 2009), pp. 339–439.

[3] M. Acet, L. Mañosa, and A. Planes, in *Handbook of Mag. Mat.*, edited by K. H. J. Buschow (Elsevier, Amsterdam, 2011), Vol. 19, pp. 231–289.

[4] A. Sozinov, N. Lanska, A. Soroka, and W. Zou, Appl. Phys. Lett. **102**, 021902 (2013).

[5] G. V. Kurdjumov, J. Metals **11**, 449 (1959).

[6] A. L. Roitburd and G. V. Kurdjumov, Mater. Sci. Eng. **39**, 141 (1979).

[7] P. J. Webster, K. R. A. Ziebeck, S. L. Town, and M. S. Peak, Philos. Mag. B **49**, 295 (1984).

[8] V. V. Martynov and V. V. Kokorin, J. Phys. III **2**, 739 (1992).

[9] J. Pons, V. A. Chernenko, R. Santamarta, and E. Cesari, Acta Mater. **48**, 3027 (2000).

[10] S. J. Murray, M. A. Marioni, S. M. Allen, R. C. O'Handley, and T. A. Lograsso, Appl. Phys. Lett. **77**, 886 (2000).

[11] O. Heczko, A. Sozinov, and K. Ullakko, IEEE Trans. Magn. **36**, 3266 (2000).

[12] A. Sozinov, A. A. Likhachev, N. Lanska, and K. Ullakko, Appl. Phys. Lett. **80**, 1746 (2002).

[13] N. Lanska, O. Söderberg, A. Sozinov, Y. Ge, K. Ullakko, and V. K. Lindroos, J. Appl. Phys. **95**, 8074 (2004).

[14] D. E. Soto-Parra, X. Moya, L. Mañosa, A. Planes, H. Flores-Zuniga, F. Alvarado-Hernandez, R. A. Ochoa-Gamboa, J. A. Matutes-Aquino, and D. Rios-Jara, Philos. Mag. **90**, 2771 (2010).

[15] T. Hickel, M. Uijttewaal, A. Al-Zubi, B. Dutta, B. Grabowski, and J. Neugebauer, Adv. Eng. Mater. **14**, 547 (2012).

[16] Q.-M. Hu, H.-B. Luo, C.-M. Li, L. Vitos, and R. Yang, Sci. China Tech. Sci. **55**, 295 (2012).

[17] P. Entel, M. Siewert, M. E. Gruner, H. C. Herper, D. Comtesse, R. Arróyave, N. Singh, A. Talapatra, V. V. Sokolovskiy, V. D. Buchelnikov *et al.*, Eur. Phys. J. B **86**, 65 (2013).

[18] V. A. Chernenko, Scr. Mater. **40**, 523 (1999).

[19] V. V. Khovaylo, V. D. Buchelnikov, R. Kainuma, V. V. Koledov, M. Ohtsuka, V. G. Shavrov, T. Takagi, S. V. Taskaev, and A. N. Vasiliev, Phys. Rev. B **72**, 224408 (2005).

[20] C. Jiang, J. Wang, P. Li, A. Jia, and H. Xu, Appl. Phys. Lett. **95**, 012501 (2009).

[21] J. Wang and C. Jiang, Scr. Mater. **62**, 298 (2010).

[22] A. Ayuela, J. Enkovaara, K. Ullakko, and R. M. Nieminen, J. Phys.: Condens. Matter **11**, 2017 (1999).

[23] V. G. Pushin, N. I. Kourov, A. V. Korolev, V. V. Marchenkov, E. B. Marchenkova, V. A. Kazantsev, N. N. Kuranova, and A. G. Popov, Phys. Solid State **55**, 2413 (2013).

[24] P. J. Brown, A. Y. Bengali, J. Crangle, K. U. Neuman, and K. R. A. Ziebeck, J. Phys.: Condens. Matter **11**, 4715 (1999).

[25] S. Fujii, S. Ishida, and S. Asano, J. Phys. Soc. Jpn. **58**, 3657 (1989).

[26] C.-M. Li, H.-B. Luo, Q.-M. Hu, R. Yang, B. Johansson, and L. Vitos, Phys. Rev. B **84**, 024206 (2011).

[27] C. Bungaro, K. M. Rabe, and A. Dal Corso, Phys. Rev. B **68**, 134104 (2003).

[28] A. T. Zayak, W. A. Adeagbo, P. Entel, and K. M. Rabe, Appl. Phys. Lett. **88**, 111903 (2006).

[29] Q.-M. Hu, C.-M. Li, R. Yang, S. E. Kulkova, D. I. Bazhanov, B. Johansson, and L. Vitos, Phys. Rev. B **79**, 144112 (2009).

[30] K. Otsuka and X. Ren, Prog. Mater. Sci. **50**, 511 (2005).

[31] T. Tsuchiya, A. Ohashi, D. Ohtoyo, H. Nakayama, M. Umemoto, and P. G. McCormick, Mater. Trans., JIM **41**, 938 (2000).

[32] D. L. Schlagel, Y. L. Wu, W. Zhang, and T. A. Lograsso, J. Alloys Compd. **312**, 77 (2000).

[33] X. Jin, M. Marioni, D. Bono, S. M. Allen, R. C. O'Handley, and T. Y. Hsu, J. Appl. Phys. **91**, 8222 (2002).

[34] J. Chen, Y. Li, J. X. Shang, and H. B. Xu, Appl. Phys. Lett. **89**, 231921 (2006).

[35] L. Vitos, *Computational Quantum Mechanics for Materials Engineers* (Springer, London, 2007).

[36] O. K. Andersen, O. Jepsen, and G. Krier, in *Lectures on Methods of Electronic Structure Calculations*, edited by V. Kumar, O. K. Andersen, and A. Mookerjee (World Scientific, Singapore, 1994), pp. 63–124.

[37] L. Vitos, H. L. Skriver, B. Johansson, and J. Kollár, Comput. Mater. Sci. **18**, 24 (2000).
[38] P. Soven, Phys. Rev. **156**, 809 (1967).
[39] L. Vitos, I. A. Abrikosov, and B. Johansson, Phys. Rev. Lett. **87**, 156401 (2001).
[40] K. Özdoğan, E. Şaşoğlu, and I. Galanakis, J. Appl. Phys. **103**, 023503 (2008).
[41] J. P. Perdew, K. Burke, and M. Ernzerhof, Phys. Rev. Lett. **77**, 3865 (1996).
[42] C.-M. Li, Q.-M. Hu, R. Yang, B. Johansson, and L. Vitos, Appl. Phys. Lett. **98**, 261903 (2011).
[43] C.-M. Li, Ph.D. thesis, School of Industrial Engineering and Management, Department of Materials Science and Engineering, KTH, Sweden, 2011.
[44] A. Ayuela, J. Enkovaara, and R. M. Nieminen, J. Phys.: Condens. Matter **14**, 5325 (2002).
[45] S. Ghosh, L. Levante, and B. Sanyal, Phys. B (Amsterdam) **406**, 2240 (2011).
[46] A. Chakrabarti, M. Siewert, T. Roy, K. Mondal, A. Banerjee, M. E. Gruner, and P. Entel, Phys. Rev. B **88**, 174116 (2013).
[47] M. Gillessen and R. Dronskowski, J. Comput. Chem. **31**, 612 (2010).
[48] C.-M. Li, H.-B. Luo, Q.-M. Hu, R. Yang, B. Johansson, and L. Vitos, Phys. Rev. B. **82**, 024201 (2010).
[49] C. P. Opeil, B. Mihaila, R. K. Schulze, L. M. nosa, A. Planes, W. L. Hults, R. A. Fisher, P. S. Riseborough, P. B. Littlewood, J. L. Smith *et al.*, Phys. Rev. Lett. **100**, 165703 (2008).
[50] P. Entel, V. D. Buchelnikov, V. V. Khovailo, A. T. Zayak, W. A. Adeagbo, M. E. Gruner, H. C. Herper, and E. Wassermann, J. Phys. D: Appl. Phys. **39**, 865 (2006).
[51] V. V. Godlevsky and K. M. Rabe, Phys. Rev. B **63**, 134407 (2001).